

## Electron-electron interaction effects on Peierls dimerization in a half-filled band

S. N. Dixit\*

*Corporate Research Science Laboratories, Exxon Research and Engineering Company, Linden, New Jersey 07036*

S. Mazumdar

*Center for Nonlinear Studies, Los Alamos National Laboratory, Los Alamos, New Mexico 87545*

(Received 6 September 1983)

A novel real-space approach to dimerization in a half-filled band is developed to investigate effects of electron-electron interactions on the Peierls instability. Dimerization is shown to be a result of imperfect resonance between pairs of electron configurations related to each other by a mirror-plane symmetry passing through the longest diagonal of the infinite ring, and the kinetic- and potential-energy contributions to the barrier to resonance are identified separately. The effects of including the on-site, nearest-neighbor, and next-nearest-neighbor interactions are investigated, and in each case it is shown that the enhancement or reduction in dimerization can be predicted from elementary physical arguments. These predictions are then substantiated by exact numerical calculations on a ten-site ring, and finite-size effects are shown to be small. The principal results that are obtained are the following: (i) The on-site correlation  $U$  strongly enhances the dimerization, the enhancement being strongest for  $U \sim 4t_0$ , where  $4t_0$  is the bandwidth of the uniform chain; (ii) the nearest-neighbor interaction  $V_1$  further enhances the dimerization until  $V_1 \leq \frac{1}{2}U$ , while  $V_1 > \frac{1}{2}U$  favors a uniform chain with a different broken-symmetry ground state, an on-site charge-density wave; (iii) for  $V_1 \leq \frac{1}{2}U$ , the second-neighbor interaction  $V_2$  reduces the dimerization slightly, although the dimerization is still stronger than that with an effective nearest-neighbor interaction  $V_1 - V_2$ ; (iv) for  $V_1 > \frac{1}{2}U$ ,  $V_2$  destroys the on-site charge-density wave and the ground state is strongly dimerized again. The complete Parisier-Parr-Pople (PPP) Hamiltonian is discussed, and it is pointed out that the above results, together with the excited-state orderings in the PPP Hamiltonian, strongly indicate that the ground state of the PPP Hamiltonian is the dimerized state. The excited-state orderings in finite polyenes, spin-density distributions in polyacetylene, and our theoretical results all indicate then that explicit inclusion of Coulomb interactions may be necessary for an accurate description of the ground and excited states in polyacetylene.

### I. INTRODUCTION

The phenomenon of Peierls instability<sup>1</sup> in partially filled one-dimensional bands has now been known for nearly 30 years. The original approach by Peierls involved a strictly one-electron model wherein phonons with wave vector  $2k_F$  couple with the band electrons to give rise to a gap at the Fermi surface of a partially filled band, where  $k_F$  is the Fermi wave vector. The energy of the occupied-band levels is lowered while that of the unoccupied levels is raised, so that there is a net gain in energy. For small distortions  $x$ , the electronic energy has a  $x^2 \ln x$  term while the elastic energy is quadratic in  $x$ , so that the system becomes unstable for an arbitrarily small electron-phonon coupling constant. Fermion-fermion interaction effects on such instabilities have been of considerable recent interest,<sup>2-14</sup> spurred on originally by the instabilities in quasi-one-dimensional charge-transfer solids and more recently by the various novel theories<sup>15-22</sup> of solitonlike and polaronlike excitations in polyacetylene.

Current theories of polyacetylene<sup>15-22</sup> usually start from the Hückel limit of zero electron correlation with an electron-phonon coupling constant modulating the nearest-neighbor transfer or resonance integral. The infinite

polyene with a half-filled band of  $\pi$  electrons is assumed to have a Peierls-dimerized ground state with an optical gap due entirely to the dimerization. Existence of such a dimerization gap in the infinite polyene was first suggested by Kuhn<sup>23</sup> as an explanation for the finite value of the optical gap that is obtained by extrapolation of optical data for long finite polyenes. While Coulson<sup>24</sup> had earlier predicted a uniform ground state for the infinite polyene, later theoretical work by Labhart,<sup>25</sup> Ooshika,<sup>26</sup> and Longuet-Higgins and Salem<sup>27</sup> indicated a dimerized ground state. Departing from the band-theory limit in the above studies, Coulson and Dixon<sup>28</sup> described dimerization within a valence-bond (VB) approach that is reminiscent of the spin-Peierls distortion. Bond-alternation domain walls were first suggested by Pople and Walmsley,<sup>29</sup> but recent excitement in this area has been generated mainly by the work of Rice<sup>17</sup> and Su, Schrieffer, and Heeger<sup>16</sup> (SSH). With few exceptions, single-particle concepts have been universally employed for polyacetylene, and direct Coulomb interactions are not fully accounted for even in the *ab initio* Hartree-Fock calculations.<sup>30</sup> Soliton excitations in polyacetylene have also been investigated within the dimerized antiferromagnetic Heisenberg spin Hamiltonian,<sup>31,32</sup> but Coulomb interactions in poly-

enes are not large enough to justify the spin model, as has been pointed out by Fukutome and Sasai.<sup>10</sup>

A completely different origin for the optical gap in the hypothetical infinite polyene was, however, proposed by Ovchinnikov and co-workers.<sup>4</sup> Electron-electron repulsion was postulated to be the principal source of the optical gap, and the ground state was predicted to have a uniform structure. Recent x-ray [Ref. 33(a)] and NMR [Ref. 33(b)] investigations on polyacetylene have definitively demonstrated the existence of a bond alternation of  $0.03 \pm 0.01 \text{ \AA}$ , thus proving the conjectures of equal bond lengths<sup>4</sup> to be incorrect. There is, on the other hand, considerable evidence of the importance of electron correlations both in the finite polyenes and in polyacetylene itself. In contradiction to the predictions of band theory, for instance, the lowest excited state in long polyenes has been determined to be a  $^1A_g$  state as opposed to the optical  $^1B_u$  state.<sup>34,35</sup> The experimental verification of this has been described in considerable detail in an excellent review by Hudson, Kohler, and Schulten.<sup>35</sup> Theoretically, polyenes of up to six and ten carbon atoms have been investigated by Ohmine *et al.*<sup>36</sup> and Soos *et al.*<sup>37</sup> within a second-quantized version of the Parisier-Parr-Pople (PPP) Hamiltonian for the  $\pi$  electrons, and a moderate to strong on-site electron correlation (Hubbard  $U$ ) was found to be essential for obtaining the correct excited-state ordering. The importance of electron correlation in polyenes has also been emphasized by Paldus, Cizek, and co-workers,<sup>38,39</sup> Matsen,<sup>40</sup> and Honig *et al.*,<sup>41</sup> among others. In the case of polyacetylene itself negative spin densities on alternate carbon atoms have recently been found.<sup>42</sup> This had previously been demonstrated for short polyene radicals,<sup>43</sup> and theoretical work had demonstrated the necessity of including electron correlation.<sup>44</sup>

Thus the nature of the ground and excited states and the origin of the optical gap in polyacetylene remains unclear, and it is of considerable importance that Coulomb interaction effects on the Peierls instability are correctly determined. Besides the potential application to polyacetylene the problem is also of fundamental interest in solid-state physics. Recent investigations in most cases have included only the on-site correlation, but even for this simplest case of the Peierls (SSH)—Hubbard model results are highly controversial. In general though, mean-field or Hartree-Fock—type approximations<sup>2-5,7,9-11</sup> predict a decrease in dimerization with an increase in Hubbard  $U$ . The ground state in the Hartree-Fock Hamiltonian is found to be a uniform spin-density-wave (SDW) state for  $U > 2t_0$ , where  $t_0$  is the transfer integral for the uniform system, as opposed to the dimerized bond-order-wave (BOW) state that occurs for smaller  $U$ .<sup>7,11</sup> Approximations which go beyond the Hartree-Fock approximation,<sup>6,8</sup> however, find a dimerized ground state at larger  $U$ , and at least in one case<sup>8</sup> actually find strong enhancement in the dimerization with  $U$ . Thus Ukrainskii<sup>6</sup> has developed a variational approach that goes beyond the generalized Hartree-Fock approach of the author and his co-workers,<sup>4</sup> and within the new approach finds a slight enhancement of the dimerization at small  $U$  followed by a smooth reduction until the limit  $U = \infty$  is reached, only at which point a uniform ground state is obtained. Second-

order perturbation theory<sup>11</sup> with the Hartree-Fock Hamiltonian as the zeroth-order Hamiltonian similarly finds an enhancement at small  $U$ , but still predicts disappearance of dimerization for  $U > 2t_0$ . Using a different perturbation technique, Horsch,<sup>8</sup> however, finds a strong enhancement of the dimerization for nonzero  $U$ . A similar enhancement was earlier found for the Peierls instability in a one-dimensional electron gas by Chui *et al.*<sup>45</sup> Numerical calculations by Jonkman, Huizinga, and Kommandeur<sup>12</sup> predict a decrease in dimerization, but as we show in the present paper, this is due to the author's limiting their calculations to a four-site, four-electron case, a Jahn-Teller distortion for which occurs at  $U = 0$ .

In contrast to the on-site correlation, few investigations of the effect of intersite interactions exist,<sup>8-10,14</sup> obviously because of the difficulty in treating short- and long-range interactions equally correctly. Even here existing results are highly contradictory. For the PPP Hamiltonian, Horsch<sup>8</sup> found the uniform ground state, and the dimerized structure could be stabilized only by assumption of a static dielectric constant strongly screening the long-range part of the interaction. The conclusion of Fukutome and Sasai<sup>10</sup> was exactly the opposite. Using an unrestricted Hartree-Fock approach, Fukutome and Sasai predicted that the on-site correlation favored the uniform structure, but long-range interactions, particularly when the less rapidly decaying parameters (Ohno parametrization) for the PPP Hamiltonian are used, strongly favor the dimerized state. Whangbo<sup>9</sup> has investigated the extended Hubbard Hamiltonian with the assumption that the nearest-neighbor interaction is strongly modulated by an electron-phonon coupling constant comparable to the one modulating the transfer integral. It was postulated that dimerization is essentially the result of such a strongly varying nearest-neighbor interaction.

No general consensus thus still exists about the effect of electron-electron interactions on the Peierls dimerization. We believe, however, that the existing perturbation results<sup>6,8,11</sup> already indicate that more correct treatments of electron correlation would find further enhancement in dimerization with  $U$ . That simple single-particle concepts will predict a decrease in dimerization with correlations can be easily seen in Fig. 1, where we show the effect of electron correlations on a one-dimensional band with a

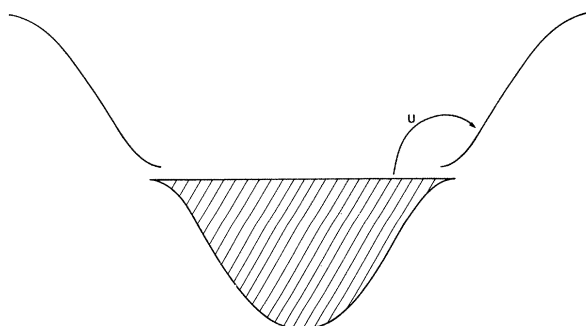


FIG. 1. Electron correlation effects on Peierls dimerization within single-particle concepts (see text).

Peierls gap. Correlations excite electrons across the Peierls gap into the hitherto unoccupied levels. Within this simplistic picture then, the energy gained on dimerization is less than that for the SSH limit. Such logic, however, is at best, incomplete, as within this picture it has been assumed from the outset that the gain in energy on dimerization is essentially kinetic. The possibility that the dimerization could be driven by the potential energy is totally neglected, and it is therefore not surprising at all that mean-field Hartree-Fock-type calculations predict a strong reduction of the dimerization. For the proper description of the correlated band, considerable departure from Peierls's one-electron picture<sup>1</sup> is required, as the band description is not valid for nonzero correlation.

The only such simple description of dimerization that is valid at all values of the correlation parameters is the double-well-potential description, as shown in Fig. 2 for the infinite polyene. Here the two degenerate dimerized phases are at the minima and the uniform structure is at the maximum. The tendency to dimerization is determined by the barrier height in the double-well potential. The effect of electron correlation can be properly determined only if the potential-energy contribution to this tunneling barrier is known. Since the double-well-potential description is essentially a real-space description, it might be anticipated that determination of the potential-energy contribution to the barrier would become simpler once a real-space view of the dimerization itself is developed.

It is the purpose of the present paper to develop such a real-space picture. A brief description of this approach has been presented previously,<sup>13</sup> where from physical arguments alone we predicted a strong enhancement of the dimerization by the on-site correlation, the enhancement being strongest for  $U \sim 4t_0$ . This was confirmed by exact numerical calculations on a Hubbard ring of six and ten sites. Finite-size effects were found to be small, as even in the worst possible case of zero dimerization and correlation, electronic energy per site of the ten-site ring was found to have converged to within 1.66% of the correct

value. Concurrently, and independently, enhanced dimerization has also been found by Hirsch,<sup>14</sup> who used a quantum Monte Carlo technique to numerically simulate a larger system. Here we take our previous real-space view of dimerization and extend our physical arguments to include the effect of both intrasite and intersite correlations. We show that a broken-symmetry wave function is necessarily the result of domination of the ground-state wave function by real-space basis functions or components which are themselves of a reduced symmetry. The variation in the tunneling barrier between the two minima in the double-well potential is analyzed separately as each new Coulomb term is added to the Hamiltonian, and in each case we show how the effect of the interactions can actually be predicted, and then substantiate our conclusions by exact numerical calculations.

There are several reasons for taking such an approach. Firstly, an exact solution of the dimerized Hubbard model using the Bethe ansatz is not possible as it is for the uniform chain,<sup>46</sup> and we have already indicated why the approximate solutions are at best incomplete. Indeed, the recent work by Hirsch<sup>14</sup> and ourselves<sup>13</sup> show that most of the conclusions based on the above approximate approaches are erroneous. On the other hand, numerical calculations, even with the Monte Carlo technique,<sup>14</sup> are limited to relatively small systems, so that a physical understanding of the dimerization process is very important. Secondly, even the most efficient numerical calculation on the largest possible system can take into account only intersite interactions  $V_j$  for which  $j < N/2$ , where  $N$  is the number of sites in the periodic ring. Since the PPP Hamiltonian contains relatively slowly decaying Coulomb terms, numerical calculations by themselves cannot be sufficient for the infinite system described by the PPP Hamiltonian. Finally, as we shall show in subsequent publications,<sup>47</sup> the present approach can be easily extended to other broken-symmetry-related problems, viz., dimerization in the  $(-A=B-)_x$  polymers<sup>48</sup> or broken-symmetry solutions in less than half-filled bands. The proof of the correctness of the reasonings lies in their ability to predict the details of the effects of every individual interaction. We investigate, in detail, the effects of the on-site, nearest-neighbor, and next-nearest-neighbor interactions here, and show that these three interactions can give rise to six possible regimes ( $U < 4t_0$ ,  $U > 4t_0$ ,  $V_1 < \frac{1}{2}U$ ,  $V_1 > \frac{1}{2}U$ ,  $V_2 > 0$  for  $V_1 < \frac{1}{2}U$ , and  $V_2 > 0$  for  $V_1 > \frac{1}{2}U$ ). In each case numerical results follow our predictions completely.

Before proceeding further we now describe the model Hamiltonian we investigate. We consider only the  $\pi$  electrons in polyacetylene and make the adiabatic approximation for the electron-phonon interactions. The model Hamiltonian  $H$  is then written in units of  $t_0$  as

$$H/t_0 = H_t + H_{el} + H_{e-e}, \quad (1a)$$

$$H_t = \sum_{i,\sigma} (1 \pm 2\alpha x) (a_{i,\sigma}^\dagger a_{i+1,\sigma} + a_{i+1,\sigma}^\dagger a_{i,\sigma}), \quad (1b)$$

$$H_{el} = 2NKx^2, \quad (1c)$$

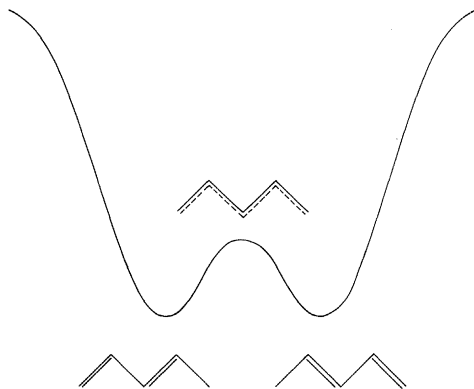


FIG. 2. Double-well-potential description of dimerization. Determination of Coulomb effects on the dimerization requires separate identifications of the potential- and kinetic-energy contributions to the tunneling barrier between the minima.

$$H_{e-e} = \frac{1}{t_0} \left[ U \sum_i n_{i\alpha} n_{i\beta} + \sum_{i,j} V_j n_i n_{i+j} \right]. \quad (1d)$$

Here  $H_t$  is the usual hopping or one-electron transfer term, with  $a_{i\sigma}^\dagger$  ( $a_{i\sigma}$ ) the creation (annihilation) operators for electrons with spin  $\sigma$ ,  $\pm x$  the atomic distortions, and  $\alpha t_0$  the electron-phonon coupling constant;  $H_{el}$  is the elastic energy, for a periodic ring of  $N$  sites with spring constant  $Kt_0$ , and  $H_{e-e}$  contains the Coulomb interaction terms. The last term is neglected in the SSH Hamiltonian.<sup>16</sup> Notice that the intersite interactions are written slightly differently from the way the PPP Hamiltonian is usually written. It is easily ascertained that this makes no difference, as the nature of the ground state is the same whether we include repulsion between electrons on singly occupied neutral carbon atoms or the attraction between  $C^+$  and  $C^-$  ions.

We now proceed to determine the effects of  $H_{e-e}$  on the dimerization. In Sec. II we first explain the diagrammatic VB notation,<sup>49</sup> and point out the relationship between the tunneling barrier in the double-well potential and the barrier to the quantum-chemical concept of resonance. We then proceed to determine the effect of the on-site correlation  $U$  on the dimerization in Sec. III. In Sec. IV we treat the intersite interactions within the same approach. We note that the present method cannot prove the existence or nonexistence of dimerization on an absolute level—in each case we can only determine whether the dimerization is enhanced or reduced as compared to the SSH Hamiltonian.<sup>16</sup> This presents no problem, as dimerization in the latter has been proved analytically.

Our principal results can be summed up as follows. (i) Hubbard  $U$  enhances the dimerization strongly,<sup>13</sup> the enhancement being largest for  $U \sim 4t_0$ , beyond which point the dimerization decreases smoothly but remains enhanced for a large range of  $U$ . (ii) The nearest-neighbor interaction  $V_1$  enhances the dimerization still further, but only as long as  $V_1 \leq U/2$ . (iii)  $V_1 > U/2$  strongly reduces the tendency to dimerization and prefers the on-site charge-density-wave (CDW) state in which alternate sites tend to be doubly occupied. (iv) For  $V_1 \leq U/2$ ,  $V_2$  has a very small effect and reduces the dimerization slightly, but the dimerization is still stronger than it is with an effective nearest-neighbor interaction  $V_1 - V_2$ . (v) For  $V_1 > U/2$ ,  $V_2$  stabilizes the dimerized structure, again very strongly. In principle, our physical arguments can be extended to more distant interactions, but in practice the situation becomes extremely complicated from  $V_3$  onwards. Similarly, the ground-state energy per site is not expected to converge at the ten-site ring when very-long-range interactions are included. We therefore do not investigate the full PPP Hamiltonian but point out that the above results are already a strong indication that the PPP ground state is dimerized for both the Mataga-Nishimoto and the Ohno parameters.

## II. VB THEORY, RESONANCE, AND DIMERIZATION

In this section we develop a real-space approach to dimerization based on a diagrammatic many-body VB formalism.<sup>49</sup> As shown schematically in Fig. 2, the system

residing at either of the two minima in the double-well potential is dimerized, while the system lying at the maximum is undimerized. Any mixing between the two dimerized states due to tunneling will reduce the dimerization. Thus the energy barrier to tunneling is a direct measure of the extent of dimerization; the larger the barrier, the less the mixing between the two dimerized states. This barrier to tunneling is intimately related to the probability of resonance between the VB diagrams that favor the BOW most strongly. Dimerization implies a lower symmetry than that of the uniform chain. The particular symmetry element that is lost upon dimerization is the mirror-plane symmetry (hereafter  $\sigma_v$ ) along the longest diagonal of the  $N$ -site ring. Application of  $\sigma_v$  on any diagram can generate the same diagram again or a different VB diagram in which the electrons are paired in a manner different from the initial diagram. Diagrams of the latter class then dominate the ground-state wave function when the system lies in either of the two minima in Fig. 2, while the wave function at the maximum is dominated by diagrams which maintain the full symmetry of the uniform chain. The uniform structure requires perfect resonance, i.e., exactly equal contributions to the ground state by each pair of diagrams related by  $\sigma_v$ . A sufficiently large barrier to resonance implies dimerization.

The strength of the present real-space approach lies in its ability to identify diagrams which favor the BOW strongly and others that favor the BOW only weakly. By analyzing the barrier to resonance between the two VB diagrams that favor the BOW most strongly, all the effects of correlation on dimerization can be predicted quite generally for arbitrarily large systems. Whether the relative contributions of all other pairs of VB diagrams related to each other by  $\sigma_v$  are equal or unequal depends only on the relative contributions of the above two extreme diagrams, since all diagrams can be generated from the extreme ones by repeated application of  $H_t$  in Eq. (1). Furthermore, the diagonal nature of  $H_{e-e}$  in the VB representation allows us to identify the kinetic- and potential-energy contributions to the barrier separately, and the effects on dimerization can then be predicted for arbitrary  $H_{e-e}$ . The influence of the on-site electron correlation on dimerization is discussed in the next section, while that of the intersite correlations is analyzed in Sec. V.

Before proceeding further we introduce the VB concepts and notations for the correlated band.<sup>49</sup> The ground state in one dimension is always a singlet (total spin  $S=0$ ), so that we shall restrict ourselves to the case where the number of up- and down-spin electrons are equal. We shall denote each doubly occupied site by a cross ( $\times$ ), an unoccupied site by a dot ( $\cdot$ ) and a pair of singlet-coupled singly occupied sites by a line or "bond" joining them. We demonstrate this for the simplest case of two electrons on two sites, the basis functions for which are as follows:

$$|\phi_1\rangle = 2^{-1/2} (a_{1,\alpha}^\dagger a_{2,\beta}^\dagger - a_{1,\beta}^\dagger a_{2,\alpha}^\dagger) |0\rangle \equiv |-\rangle, \quad (2)$$

$$|\phi_2^\pm\rangle = 2^{-1/2} (a_{1,\alpha}^\dagger a_{1,\beta}^\dagger \pm a_{2,\alpha}^\dagger a_{2,\beta}^\dagger) |0\rangle \\ = 2^{-1/2} \{ |\times \cdot\rangle \pm |\cdot \times\rangle \}. \quad (3)$$

Spatial symmetry allows us to further classify the  $S=0$

subspace into an  $A$  subspace (plus linear combination of diagrams) and a  $B$  subspace (minus linear combination). The ground state is in the  $A$  subspace and consists of  $|\phi_1\rangle$  and  $|\phi_2^+\rangle$  while the  $B$  subspace consists only of  $|\phi_2^-\rangle$ . Optical absorption from the ground state can only occur to the  $B$  subspace, as can be seen from the nature of the velocity operator

$$\vec{v} = \frac{ita}{\hbar} \sum_{i,\sigma} (a_{i,\sigma}^\dagger a_{i+1,\sigma} - a_{i+1,\sigma}^\dagger a_{i,\sigma}). \quad (4)$$

The situation with larger systems is slightly more complicated. Bonds are not restricted to nearest neighbors and long non-nearest-neighbor bonds are created.<sup>49</sup> We illustrate this with  $N=4$ . The simplest basis functions here are products of functions of the type in Eqs. (2) and (3). We choose the function

$$|\psi_1\rangle = 2^{-1} (a_{1,\alpha}^\dagger a_{2,\beta}^\dagger - a_{1,\beta}^\dagger a_{2,\alpha}^\dagger) (a_{3,\alpha}^\dagger a_{4,\beta}^\dagger - a_{3,\beta}^\dagger a_{4,\alpha}^\dagger) |0\rangle$$

$$\equiv \text{---} \quad \text{---} \quad , \quad (5)$$

and apply  $H_t$  between the nonbonded sites 2 and 3. This generates the functions

$$|\psi_2\rangle = 2^{-1/2} a_{2,\alpha}^\dagger a_{2,\beta}^\dagger (a_{1,\alpha}^\dagger a_{4,\beta}^\dagger - a_{1,\beta}^\dagger a_{4,\alpha}^\dagger) |0\rangle$$

$$\equiv \text{---} \overset{\text{x}}{\cdot} \text{---} \quad (6a)$$

and

$$|\psi_3\rangle = 2^{-1/2} a_{3,\alpha}^\dagger a_{3,\beta}^\dagger (a_{1,\alpha}^\dagger a_{4,\beta}^\dagger - a_{1,\beta}^\dagger a_{4,\alpha}^\dagger) |0\rangle$$

$$\equiv \overset{\cdot}{\text{---}} \text{---} \text{x} \quad (6b)$$

Back transfer now leads to the same function  $|\psi_4\rangle$  in both cases, given by

$$|\psi_4\rangle = 2^{-1} (a_{1,\alpha}^\dagger a_{4,\beta}^\dagger - a_{1,\beta}^\dagger a_{4,\alpha}^\dagger) (a_{2,\alpha}^\dagger a_{3,\beta}^\dagger - a_{2,\beta}^\dagger a_{3,\alpha}^\dagger) |0\rangle$$

$$\equiv \text{---} \text{---} \quad (7)$$

All possible diagrams can be generated in this manner for arbitrary large systems by joining the singly occupied sites in every possible manner, but with one restriction: only nested (i.e., noncrossing) bonds are allowed. Diagrams in which two or more bonds cross can be shown to be linearly dependent on other diagrams.<sup>49</sup> There are thus only two diagrams in the  $N=4$  chain which do not possess doubly occupied sites, as can be seen from Eqs. (5) and (7). Both these diagrams occur in the  $A$  subspace, so that the optical  $B_u$  state consists of diagrams that possess at least one doubly occupied site. Thus for nonzero  $U$  the optical gap is  $\sim U$  while the lowest excited state in the  $A$  subspace still has contributions from diagrams which involve singly occupied sites only and in the limit of  $U \rightarrow \infty$  occurs at  $\sim 4t_0^2/U$ . For all chain lengths  $N \geq 4$  the  $A$  subspace always contains an excess of such "covalent" diagrams, and the occurrence of the  ${}^1A_g$  excited state below the  ${}^1B_u$  state in long polyenes thus necessarily implies a moderate to large  $U$  ( $U > 2t_0$ ). Note that this observation follows naturally from the symmetry of the VB basis functions, whereas the molecular-orbital or band approach requires an actual tedious configuration interaction calculation. We shall show below that the dimerization problem can also be analyzed very simply using this real-space

approach.

For the dimerization problem we have to consider the infinite chain, representative diagrams for which are shown in Fig. 3. Diagrams will be called covalent if the number of crosses  $N_x=0$ , while diagrams with  $N_x \neq 0$  will be referred to as ionic. The two covalent diagrams  $|I\rangle$  and  $|II\rangle$  with only nearest-neighbor bonds will be termed as Kekulé structures, while covalent diagrams with at least one non-nearest-neighbor bond will be called Dewar structures. The total number of VB diagrams  $N_T$  for a  $N$ -site half-filled system is given by

$$N_T = \sum_{N_x=0}^{N/2} \binom{N}{N_x} \binom{N-N_x}{N-2N_x} \frac{(N-2N_x)!}{(N/2-N_x)!(N/2-N_x+1)!}, \quad (8)$$

so that even after use of spatial and electron-hole symmetry<sup>37</sup> the dimension of the Hamiltonian matrix grows very rapidly ( $N_T=2760615$  for  $N=14$ ) and actual numerical calculations quickly became impossible. On the other hand, Hartree-Fock-type calculations based on single-particle concepts are bound to yield erroneous results as  $U$  increases. What is therefore required is a physical understanding of the dimerization process itself so that Coulomb effects can actually be predicted, exactly as the occurrence of the  ${}^1A_g$  state below the  ${}^1B_u$  can be predicted.

A dimerized or BOW state implies periodic modulation of the ground-state bond orders, where the bond order  $P_{i,i+1}$  between sites  $i$  and  $i+1$  is defined as

$$P_{i,i+1} = \frac{1}{2} \left\langle \sum_{\sigma} a_{i,\sigma}^\dagger a_{i+1,\sigma} + a_{i+1,\sigma}^\dagger a_{i,\sigma} \right\rangle. \quad (9)$$

From Eq. (9), a difference in the bond orders  $P_{i,i+1}$  and  $P_{i-1,i}$  requires a difference in the probabilities of charge transfers between sites  $i$  and  $i+1$  and between sites  $i$  and  $i-1$ . If site  $i$  is singly occupied, the largest difference in bond orders occurs when only *one* of the two sites  $i \pm 1$  is occupied by a single electron with the same spin as the one in site  $i$ . If the other site is empty a single charge transfer *from*  $i$  can occur, while if it is doubly occupied, charge transfer *to*  $i$  is allowed. Only if the other site is occupied by a single electron that has a spin opposite to that at  $i$ , can both charge transfers to and from  $i$  occur. Thus the difference between  $P_{i,i+1}$  and  $P_{i,i-1}$  is largest when one of

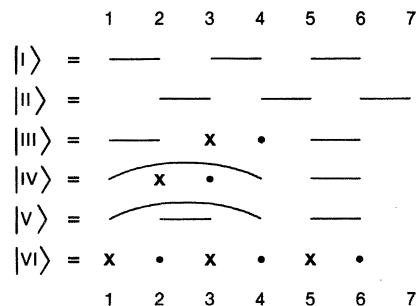


FIG. 3. Finite segments of representative VB diagrams (see text) for a half-filled band. Site indices have been included at the top and the bottom.

two sites  $i \pm 1$  is occupied by a single electron whose spin is parallel to the electron occupying  $i$  while the other is occupied by a single electron with opposite spin. If we now consider the case where site  $i$  is doubly occupied, similar arguments can be made to show that in this case the difference between  $P_{i,i+1}$  and  $P_{i-1,i}$  is largest when one of the sites  $i \pm 1$  is also doubly occupied but the other is empty. We need not consider the possibility that site  $i$  can be empty, as this is related by electron-hole symmetry to the case where  $i$  is doubly occupied. The infinite-chain wave function is a linear combination of many configurations, each of which may have the above local arrangements. Configurations in which these arrangements can occur have a lower symmetry than the infinite periodic ring, and dimerization occurs when any two configurations related by  $\sigma_v$  make unequal contributions to the ground-state wave function, i.e., resonance is imperfect. For the dimerization problem then, we are interested in determining which pair of configurations favor the BOW most strongly, as well as the barrier to resonance between these configurations.

Having determined which local arrangements of electrons favors the largest difference in  $P_{i,i+1}$  and  $P_{i-1,i}$ , we note that the  $N$ -site configurations that favor the BOW most strongly must have these arrangements repeated throughout the length of the infinite ring. We first focus on the repeat unit in which the central atom is singly occupied and differences in bond orders occur due to spin dependence of  $H_t$ . Each VB diagram in Fig. 3 is a linear combination of many configurations. Bonded sites necessarily have opposite spins while nearest-neighbor nonbonded sites have parallel and opposite spins with equal probability, so that a given diagram favors greater charge transfer between singly occupied bonded sites than between singly occupied nonbonded sites. In Fig. 3, for instance, the matrix element of  $H_t$  between  $|I\rangle$  and  $|III\rangle$  is 1 in units of  $t_0$  near  $\alpha \rightarrow 0$  while  $\langle I|H_t|IV\rangle$  has a factor of  $\frac{1}{2}$ .  $|I\rangle$  therefore favors greater charge transfer between sites 3 and 4 than between sites 2 and 3. The Kekulé diagram  $|II\rangle$ , on the other hand, favors larger transfer between sites 2 and 3. It can also be seen that both Kekulé diagrams have a lower symmetry than the periodic ring, and each is related to the other by  $\sigma_v$ . To determine which diagrams favor the BOW most strongly we classify bonds between sites  $i$  and  $i+1$  as even if  $i$  is even and odd otherwise, and define  $\delta$  to be the difference between the total numbers of even and odd bonds within any diagram. From what we have already said, VB diagrams with a large  $|\delta|$  favor the BOW most strongly, as these maintain the phase of the BOW throughout the infinite ring. Long non-nearest-neighbor bonds, as in the Dewar structures, reduce  $|\delta|$  considerably as these destroy two neighboring even (odd) bonds and create an odd (even) bond at their expense. We have, in effect, assigned "left" and "right" characters to the basis functions. Since the replacement of two nearest-neighbor short bonds with a long bond and an enclosed short bond reverses the character of the latter,  $|\delta|$  decreases in general with the lengths and numbers of non-nearest-neighbor bonds. For the covalent structures then,  $|\delta|$  is largest for the two Kekulé structures  $|I\rangle$  and  $|II\rangle$  ( $|\delta| = N/2$ ).

Classifying diagrams in terms of  $N_x$ , we see that an increase in  $N_x$  rapidly decreases  $|\delta|$  due to two reasons. Firstly, of course, the overall probability of having bonded sites itself decreases as more and more bonds are replaced by a cross and a dot. More importantly, creation of empty sites increases the probability of having non-nearest-neighbor bonds, thus reducing  $|\delta|$  more drastically. Thus irrespective of system size, the Kekulé structures always have the largest  $|\delta|$ , even when ionic diagrams are taken into consideration.

An important condition for dimerization that emerges from the above is that *if the ground state is dominated by diagrams with large  $|\delta|$ , dimerization will occur while a ground state dominated by diagrams with  $\delta \rightarrow 0$  may favor a uniform bond order.*

We digress here to point out that these considerations are sufficient to explain the difference between finite and infinite  $(4n+2)$ -electron rings on the one band and one of the differences between finite  $4n$ - and  $(4n+2)$ -electron rings on the other hand. Previous explanations have been based on the  $U=0$  band picture only.<sup>11</sup> For finite systems covalent diagrams make a large contribution to the ground-state wave function even for  $U=0$ . For the  $(4n+2)$ -electron rings, there are  $2n+1$  bonds in the covalent diagrams, so that it is always possible to have at least one long non-nearest-neighbor bond and an equal number of even and odd bonds. The number of such Dewar diagrams with  $\delta=0$  can be found very easily. Once the long bond is drawn, there are then  $n$  ways of having  $\delta=0$ , the number of pairs of odd and even bonds going from 1 to  $n$ . Application of  $(2n+1)$ -fold rotational symmetry will generate all possible such diagrams and the total number of covalent diagrams with  $\delta=0$  is then  $(2n+1)n$ . The fraction  $f$  of covalent diagrams that have  $\delta=0$  is therefore given by

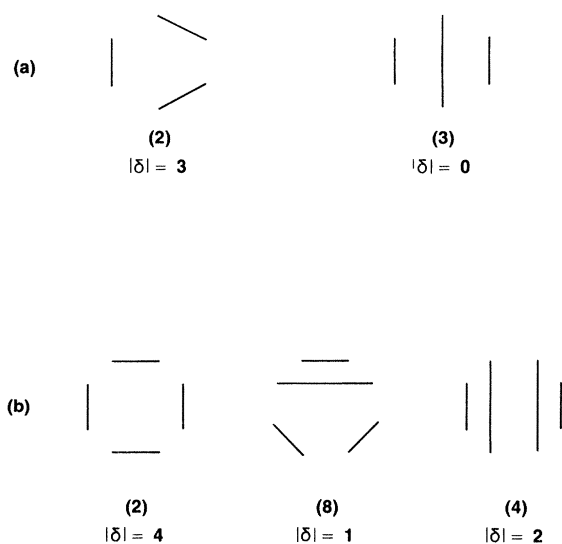


FIG. 4. Covalent diagrams with the corresponding values of  $|\delta|$  for (a)  $N=6$ , and (b)  $N=8$  site rings. Numbers in parentheses represent the total number of diagrams of each kind that can be generated by rotation.

$$f_{4n+2} = (2n+1)n \frac{(2n+1)!(2n+2)!}{(4n+2)!} \quad (10)$$

In Fig. 4(a) we present the two kinds of covalent diagrams for  $N=6$  along with the corresponding values of  $|\delta|$ . The numbers in parentheses denote the total number of diagrams that can be generated by rotations. For small  $(4n+2)$ -electron rings then, a very large fraction  $f_{4n+2}$  of the covalent diagrams favor the uniform bond order. However,  $f_{4n+2}$  decreases rapidly with  $n$  ( $f = \frac{3}{5}$  for  $n=1$ ,  $\frac{10}{42}$  for  $n=2$ ,  $\frac{21}{429}$  for  $n=3$ , etc.) approaching 0 for  $n \rightarrow \infty$ , thus implying that the uniform structure becomes less and less stable as the size increases.

With the  $4n$ -electron rings on the other hand, the situation is entirely different. There are now  $2n$  bonds possible in the covalent diagrams, so that there is no way to construct a long non-nearest-neighbor bond and still have equal numbers of even and odd bonds. Construction of an even number of long bonds changes the character of the short bonds an even number of times, so that such diagrams cannot have  $\delta=0$  either. The fraction  $f_{4n}$  is then zero, as all covalent diagrams favor a BOW. This is shown in Fig. 4(b) for  $N=8$ ,  $N=4$  being trivial in the sense that only Kekulé structures with  $|\delta|=2$  are possible. Notice that although the last set of diagrams in Fig. 4(b) resembles the Dewar diagram for  $N=6$ , here both the nearest-neighbor bonds are either even or odd. The smallest  $4n$ -electron systems are then dimerized for arbitrarily small  $\alpha$ . The size dependence of the tendency to dimerization is also opposite for  $4n$ - and  $(4n+2)$ -electron systems, as can be seen by comparison of  $|\delta|/N$  for  $N=4$  and 8 for instance. In the  $4n$ -electron rings, diagrams with smaller and smaller  $|\delta|/N$  occur as  $N$  increases and the tendency to dimerization *decreases* here with size, unlike the  $(4n+2)$ -electron rings.

Until now we have considered only the spin dependence of  $H_t$  and the difference in bond orders that arises from this spin dependence. We now consider the repeat unit consisting of doubly occupied sites. From our classifications of bonds as even or odd, highly ionic diagrams that favor a BOW must have an even number of crosses distributed over consecutive even number of sites. If on both sides of such a segment we have unoccupied sites, the bonds that can be formed by charge transfer are either both even or odd. On the other hand, if we consider a segment consisting of an odd number of crosses, one of the two bonds that can be formed on either side is odd while the other is even. The two configurations that favor the BOW most strongly, as far as the occupancy dependence of  $H_t$  is considered, are, therefore, the ones that have the occupancy schemes  $\cdots 00220022 \cdots$  and  $\cdots 22002200 \cdots$ , where the numbers 2 and 0 denote doubly occupied and empty sites respectively. We now have to decide which particular pair of VB diagrams, the Kekulé structures or the above pair of ionic diagrams with  $N_x = N/2$ , favor the BOW more strongly.

In any  $(4n+2)$ -electron ring the maximum number of doubly occupied sites is  $2n+1$ , so that there is always at least one segment consisting of an odd number of doubly occupied sites in diagrams with  $N_x = N/2$ . Around this segment equal bond orders are preferred, so that with the

$(4n+2)$ -electron systems the Kekulé structures are the ones that favor the BOW most strongly. This difference between the Kekulé structures and the highly ionic diagrams is real and independent of the actual size of the system since each diagram close to the Kekulé structures favors the BOW more strongly than a diagram equally close to the highly ionic diagrams. For the  $(4n+2)$ -electron systems then we need to consider the barrier to resonance between the Kekulé structures only to determine correlation effects.

For the  $4n$ -electron systems the maximum number of doubly occupied sites is  $2n$ , so that it is always possible to have diagrams with  $N_x = N/2$  that contain isolated segments consisting of even numbers of doubly occupied sites only. This second difference between  $4n$ - and  $(4n+2)$ -electron systems is shown in Fig. 5. For  $N=6$ , only the last two kinds of diagrams favors a BOW, but relative to the Kekulé structures, they favor it only weakly as the single isolated cross favors equal bond orders on both sides. For  $N=4$  the second set of diagrams favor the BOW as strongly as the Kekulé structures. In the  $4n$ -electron systems then dimerization is favored equally by the Kekulé structures and the pair of highly ionic configurations  $\cdots 00220022 \cdots$  and  $\cdots 22002200 \cdots$ . The effect of the on-site correlation on the dimerization in  $4n$ -electron systems is immediately obvious. For  $U > 0$  the relative weights of the above two ionic diagrams decrease continuously while those of the Dewar structures increase, so that the tendency to dimerization decreases with  $U$ . Within the band-theoretical approach, the degeneracy at the Fermi level gives a Jahn-Teller distortion, but a  $U > 0$  decreases the probability of this zeroth-order configuration. This explains then why Jonkman *et al.*<sup>12</sup> find a decrease in dimerization with  $U$  in a ring of four electrons. We have thus shown how the differences in behavior between  $4n$ - and  $(4n+2)$ -electron systems arise from real-space topological considerations, and depend only on whether the number of ways electrons may be paired as bonds or crosses is even or odd. Finite  $4n$ -electron rings which exhibit a Jahn-Teller distortion are not suitable systems for investigating correlation effects and throughout the rest of our discussion we shall consider the  $(4n+2)$ -electron rings only.

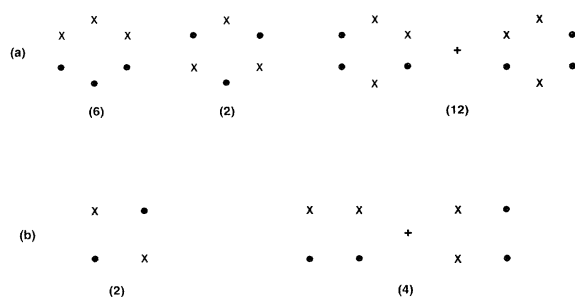


FIG. 5. Ionic diagrams with  $N/2$  doubly occupied sites for  $N=6$  and 4. Numbers in parentheses have the same meaning as in Fig. 4. Second set of ionic diagrams for  $N=4$  favors the BOW as strongly as the Kekulé diagrams for this case.

### III. EFFECTS OF THE ON-SITE CORRELATION ON DIMERIZATION

Having established that in the  $(4n+2)$ -electron rings the Kekulé diagrams favor the BOW most strongly, we now proceed to determine the kinetic- and potential-energy contributions to the barrier to resonance between these in the presence of nonzero Hubbard  $U$ . The probability of resonance between any two diagrams related by  $\sigma_v$  depends essentially on the ease with which each diagram may be converted to the other. We start from diagram  $|I\rangle$  in Fig. 3 and apply  $H_t$  repeatedly until we reach  $|II\rangle$ . At each step after the initial creation of a cross and a dot there are two possibilities, a cross or a dot can move to the left or right or a new pair of cross and dot may be created. Such bifurcations lead to many possible paths between the Kekulé diagrams, involving all possible diagrams. For illustration, a few representative paths for  $N=6$  are shown in Fig. 6. Each path may be characterized by the largest  $N_x$  involved. It should be obvious that similar paths may be constructed for arbitrary  $N$ , the minimum number of steps in each path being  $N$ . A uniform ground state with equal bond orders requires equal contributions from the two Kekulé diagrams and all pairs of diagrams symmetrically related to these. The barrier to resonance increases with the lengths of the paths (system size<sup>28</sup>) and decreases with the number of possible paths, all paths being equally probable at  $U=0$ . Since only  $H_t$  connects two consecutive VB diagrams along any path, the length of the paths is a direct measure of the kinetic-energy contribution to the barrier to resonance. Paths are sufficiently long for the infinite system so that the kinetic-energy contribution alone can give rise to dimerization at  $U=0$ . For  $U>0$  there is an additional

potential-energy contribution to the barrier, as seen in Fig. 6. Paths involving  $N_x$  doubly occupied sites now cost an extra energy  $N_x U$ . Paths involving large  $N_x$  become highly unfavorable for  $U>0$ , so that the overall barrier to resonance rises considerably. A positive  $U$  is therefore expected to enhance the dimerization.

Since all  $P_{i,i+1}$  go to zero, however, at  $U \rightarrow \infty$ , we expect a reversal in the enhancement effect at some  $U_{\text{rev}}$ . The reversal effect is associated with the virtual transfers in which an electron hops from site  $i$  to  $i+1$ , creates a double occupancy at site  $i+1$ , and then one of the two electrons at  $i+1$  hops back to site  $i$ . If the electron at site  $i$  is now the one which originally occupied  $i+1$ , bonding schemes are severely altered. Such virtual transfers can thus destroy two neighboring even (odd) bonds and create an odd (even) bond and a non-nearest-neighbor bond at their expense, strongly reducing  $|\delta|$ . In Fig. 3, for instance, virtual transfers between sites 2 and 3 in  $|I\rangle$  lead to  $|V\rangle$ ,  $|\delta|$  for which is smaller than that of  $|III\rangle$ , which is reached by real transfer from  $|I\rangle$ . Thus paths involving virtual transfers and covalent diagrams only can also be constructed between  $|I\rangle$  and  $|II\rangle$ , exactly in the manner of Fig. 6. Each step in paths involving virtual transfers involves shifting a bond instead of an electron, so that there are only  $N/2-1$  steps in these paths, as opposed to  $N$  steps in Fig. 6. For  $N=6$ , for example, paths involving virtual transfers have only one intermediate diagram, one of the three Dewar structures in Fig. 4(a). The dimerization is therefore reduced when these paths are favored over the ones in Fig. 6. The necessary condition for the above is that the net contribution of the covalent diagrams to the ground-state wave function, starting from the asymptotic value of zero at  $U=0$ , is larger than the total contributions by the ionic diagrams. The magnitude

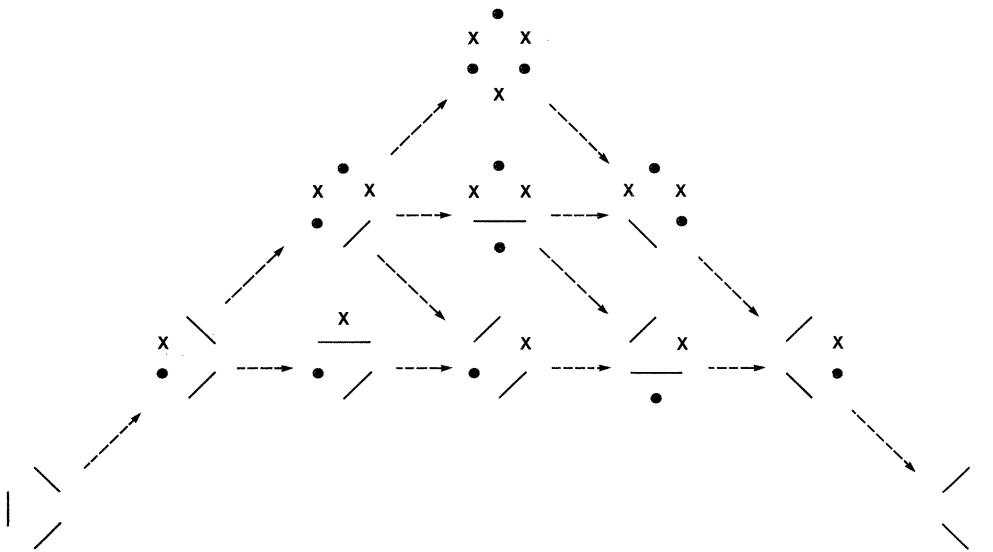


FIG. 6. Representative paths in configuration space connecting the two Kekulé diagrams. Pairs of consecutive diagrams are related by the hopping term  $H_t$  in Eq. (1).

of  $U$  at which this occurs can be obtained from the exact expression for the optical gap in the undimerized Hubbard Hamiltonian. In the large- $U$  limit, the optical gap, the minimum energy for a real transfer is  $U - 4t_0 + (8t_0^2/U)\ln 2$ , and for very large  $U$  the ground state is composed of covalent diagrams only. The minimum value of  $U$  at which the covalent diagrams dominate the wave function and the Heisenberg spin Hamiltonian begins to be valid approximation is the smallest  $U$  for which the above large- $U$  expression for the optical gap is valid, viz.,  $U \sim 4t_0$ . Thus for  $0 \lesssim U \lesssim 4t_0$  we expect a strong enhancement of the dimerization, while from  $U \sim 4t_0$  onwards the dimerization should decrease smoothly, although relative to  $U=0$  dimerization may be enhanced for a large range of  $U$ , since paths involving real transfers are still not totally forbidden.

We have performed exact numerical calculations for the finite rings  $N=6$  and  $10$  to verify the above conclusions. These involved all possible VB diagrams in both cases, 175 for  $N=6$  and 19404 for  $N=10$ . We use the rotational symmetry element  $C_{N/2}$ , the mirror-plane symmetry  $\sigma_V$  that lies between the atoms and the electron-hole symmetry,<sup>37</sup> and computer-generate all linear combinations of the VB diagrams that form the complete set of basis functions for the Hamiltonian. The use of the above symmetry elements reduces the dimensions of the Hamiltonian matrix to 27 for  $N=6$  and 1114 for  $N=10$ . Each basis function is diagonal in  $H_{e-e}$  and operation on each of them with  $H_t$  generates a finite number of other functions. Overlaps between the various basis functions are calculated exactly and these are then used to numerically calculate the exact ground-state energies and wave functions from the Hamiltonian matrix as a function of the correlation parameter and  $\alpha x$ . The  $N=14$  system with 2760715 diagrams is currently beyond our reach. Unlike the infinite system, finite rings exhibit dimerization only for  $\alpha$  greater than certain  $N$ -dependent threshold values. However, the effect of  $U$  is local and the behavior of finite systems near the threshold  $\alpha$  should mimic the behavior of the infinite system with an infinitesimally small electron-phonon coupling constant.<sup>50</sup> As we point out later, ground-state electronic energies per site have essentially converged at  $N=10$  for all  $U$  and  $\alpha x$ . To make the difference between  $U=0$  and  $U>0$  most conspicuous we choose in each case  $\alpha^2/K$  just below the threshold value such that the system is undimerized for  $U=0$ . For  $\alpha$  much larger than this the smaller transfer integral becomes too small and spin exchange (virtual transfer) becomes important too soon, so that the actual effect of  $U$  is lost. For each  $U$  then, we calculate the exact total energy, electronic plus elastic,  $E(U, \alpha x)$ , and the stabilization energy gained per electron on dimerization,

$$\frac{\Delta E}{Nt_0} = \frac{1}{Nt_0} [E(U, \alpha x) - E(U, 0)]. \quad (11)$$

We have been able to reproduce the  $N=6$  results for the three values of  $U/t_0$  studied earlier.<sup>11</sup> However, the  $\Delta E$  calculated here is defined differently to make the comparison between various  $U$ 's more straightforward. In Figs. 7(a) and 7(b) we present our results for the two cases. In each case we plot  $\Delta E/Nt_0$  against  $\alpha x$  for several values

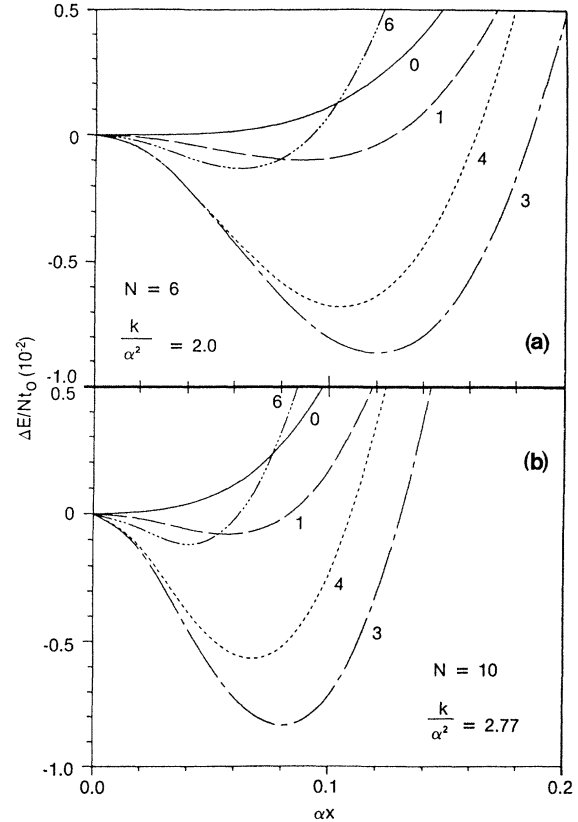


FIG. 7. Energy gained per electron on dimerization for the six- and ten-membered rings. Numbers on each curve are the different values of  $U/\sqrt{2}t_0$ .

of  $U/t_0$ . The strong enhancement of the dimerization for  $U/\sqrt{2}t_0 \lesssim 3$  and the smooth decrease of the enhancement factor beyond this point are obvious in both cases. The exact reversal points where the enhancement factors begin to decrease are  $U/\sqrt{2}t_0 = 3.5 \pm 1$  for  $N=6$  and  $3.1 \pm 0.1$  for  $N=10$ .

The nearly identical results for  $N=6$  and  $10$  indicate that the present arguments are correct and finite-chain effects are small. Unlike the excitation energies, the ground-state electronic energy per site can be expected to converge rather fast with increase in system size. Convergence here may be checked most easily by comparing the energy densities of the  $N=6$  and  $10$  rings with that of the infinite system for the two cases, (i)  $U=0, \alpha x \neq 0$  and (ii)  $U \neq 0, \alpha x = 0$ . Thus the difference in energy densities between the  $N=10$  ring and the infinite chain at  $U=0$  and  $\alpha x = 0$  and  $0.1$  are 1.66% and 0.5%, respectively, of the true values. Indeed such comparisons of the  $U=0, \alpha x \neq 0$  energies in Fig. 8 indicate that even for  $U=0$ , where convergence is slowest, the energy densities of the  $N=10$  ring are much closer to those of the infinite system than to those of  $N=6$ . The energy densities of the undimerized Hubbard systems<sup>46</sup> are also plotted in Fig. 8, and the negligible finite-chain effects are again obvious. Once again the  $N=10$  ring is found to be closer to the infinite system than to  $N=6$ , indicating the very rapid convergence. Convergence is even faster when both  $U$  and  $\alpha x$

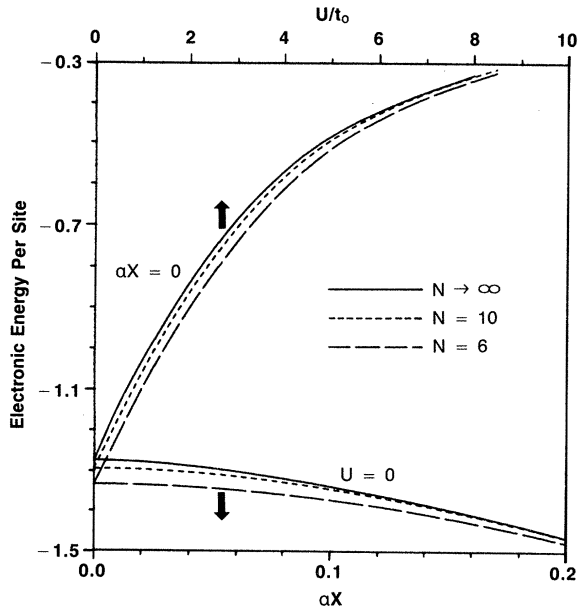


FIG. 8. Ground-state electronic energies per site for  $U=0, \alpha x > 0$  and  $U > 0, \alpha x = 0$  for  $N=6, 10$ , and the infinite chain (Ref. 46).

are nonzero, so that the  $N=10$  results are always within 1–1.5% of the true values and reproduce the behavior of the infinite chain far better than any of the previous approximate approaches, especially for  $U > 2t_0$ , where localization due to correlations is very important. The only difference between finite and infinite systems is then that dimerization is conditional in the finite systems due to the short lengths of the paths between the Kekulé structures. This is of no concern here, as we are interested only in the relative differences between various  $U$  and the existence of the dimerized state for  $U=0$  has already been proved.

To demonstrate the intimate relationship between the change in the nature of the *undimerized* wave function and the actual magnitude of  $U_{\text{rev}}$  we have also calculated the exact wave functions. We classify VB diagrams according to  $N_x$  and determine the total normalized contributions of each class to the ground-state wave function. At  $U=0$  and for a  $(4n+2)$ -electron ring the contributions are largest for the two classes of diagrams characterized by  $N_x=n$  and  $n+1$ . The contributions of all other classes are symmetric around these two and are infinitesimally small for  $N_x=0$  and  $2n+1$ . In Fig. 9 we present the contributions of the six classes of diagrams for  $N=10$  as a function of  $U/\sqrt{2}t_0$ . The lines are drawn between the points only to guide the eye, but similar continuous curves would be obtained in the limit  $N \rightarrow \infty$ . The peaks in the curves shift towards smaller and smaller  $N_x$  with increase in  $U$ , and only for  $U/\sqrt{2}t_0 > 3$  is the contribution of the covalent diagrams larger than that of any other class. Together with the results of Fig. 7, this then completes the verification of our prediction that  $U_{\text{rev}} \sim 4t_0$ . This shifting of the peak towards smaller  $N_x$  is intimately related to enhancement in the dimerization, as it signifies a larger barrier to resonance in Fig. 6. On the other hand, the

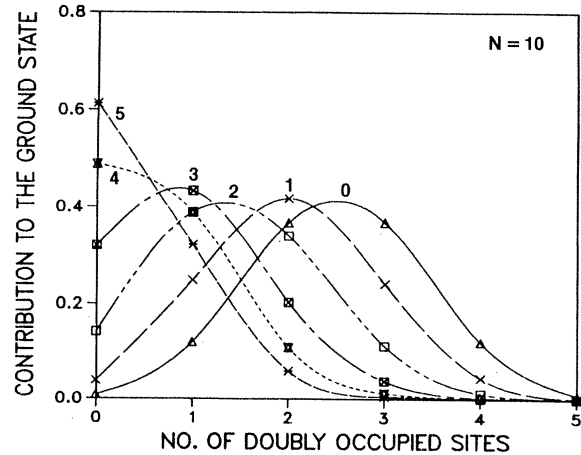


FIG. 9. Total normalized contributions to the undimerized ground-state wave function by the various classes of diagrams with fixed number of doubly occupied sites. Curves are drawn to guide the eye and the numbers against these are the values of  $U/\sqrt{2}t_0$ .

pure SDW phase represents a  $\delta$  function at  $N_x=0$ , and once the peak is at  $N_x=0$  further increase in  $U$  only decreases the dimerization.

We now discuss an additional feature of the correlated wave function as seen in Fig. 9. It has been claimed from Hartree-Fock calculations<sup>11</sup> that the Peierls-Hubbard Hamiltonian can be approximated by an effective SSH Hamiltonian with a dressed electron-phonon coupling constant  $\alpha_{\text{eff}}$ . The electron-phonon coupling constant distinguishes between diagrams related by  $\sigma_y$  (the two Kekulé diagrams for instance) but makes no distinction between diagrams with different  $N_x$ . For the SSH Hamiltonian, the  $U=0$  relative weights in Fig. 9 remain unaltered for arbitrary  $\alpha$ . Thus while the expectation value  $\langle n_{i\alpha} n_{i\beta} \rangle$  changes continuously with  $U$ , it remains essentially fixed at 0.25 for the SSH Hamiltonian. This then implies that correlation effects can never actually be approximated by an  $\alpha_{\text{eff}}$ , even at small values of  $U$  where Hartree-Fock calculations might yield nearly correct energies.

To summarize the present section then, a nonzero  $U$  is a barrier to resonance and as such is the driving force behind the dimerization.<sup>13</sup> This remains true until  $U$  is so large that the ground-state wave function is dominated by Dewar structures with long bonds, as in the Heisenberg antiferromagnetic chain. The path formulation of resonance introduced in this context is very similar to that of Coulson and Dixon,<sup>28</sup> who, however, considered the covalent diagrams only and were interested in what is commonly known as spin-Peierls transition. Similar concepts have also been used in the context of three-dimensional antiferromagnetism by Anderson,<sup>51</sup> and indeed, are characteristics of all broken-symmetry-related problems. As we demonstrate in the next section, this single concept is sufficient to predict and understand the effects of nonzero intersite interactions, and, in principle, could be extended to cases where the range of interactions is arbitrarily long.

#### IV. EFFECTS OF INTERSITE INTERACTIONS

As already discussed in Sec. I, relatively little interest has been paid to the role of intersite Coulomb interactions. The PPP Hamiltonian consists of large intersite interactions and their effects on the dimerization could also be very strong. Furthermore, within the Peierls (SSH)—Hubbard model the only competition is between the uniform SDW state and the dimerized BOW state. Nonzero intersite interactions can make a third kind of state important, viz., the on-site CDW state, which, while favoring equal spin densities on sites, will strongly oppose dimerization. This will be particularly important in this commensurate case of the half-filled band where the phases of the two different kinds of charge-ordered states are distinct. An earlier discussion of these two different kinds of states may be found in the work by Paldus and Cizek.<sup>38</sup>

Even with the few existing studies, results are mutually contradictory, as pointed out in Sec. I. The conclusions of Fukutome and Sasai<sup>10</sup> and Horsch<sup>8</sup> are exactly opposite and the probable reason for this is as follows. Fukutome and Sasai<sup>10</sup> investigate the PPP Hamiltonian within an unrestricted Hartree-Fock approach, which, as we have already shown, may lead to erroneous results. Horsch,<sup>8</sup> on the other hand, treats the intersite interactions within a mean-field-type approximation in which the nearest-neighbor interactions are incorporated within an effective hopping integral, the implication of which then would be that the PPP Hamiltonian can be approximated by an effective Hubbard Hamiltonian with a modified spring constant. We shall show in the present section that the above is also incorrect. Whangbo<sup>9</sup> and Hirsch<sup>14</sup> have investigated the effect of the nearest-neighbor interaction within an extended Hubbard Hamiltonian. In Whangbo's model the dimerization arises principally from an electron-phonon coupling constant modulating the nearest-neighbor interaction, while Hirsch finds a strong enhancement of the dimerization with the nearest-neighbor interaction that is independent of the distance between neighboring atoms. We shall show that Hirsch's results are not only correct, but can indeed be predicted for the extended Hubbard model provided the nearest-neighbor interaction is smaller than an upper limit. Dimerization is progressively enhanced only for a nearest-neighbor interaction  $V_1 \lesssim U/2$ , and is strongest for  $V_1 = U/2$ .

In the present section we deal with each Coulomb term individually, and consider the enhancement or reduction of dimerization in each case within the same framework of Sec. II. In each case the effect on the dimerization can be predicted from the increase or decrease in the barrier to resonance. Furthermore we show that while in most cases electron correlations strongly enhance the dimerization, the nature of the ground state also depends strongly on the *relative magnitude* of the correlation parameters, so that in certain cases correlations can destroy the dimerized state and favor uniform bond order. We discuss the several possible cases below and consider only repulsive interactions as in Eq. (1a). The reason for this has already been given in Sec. I.

#### A. $V_1 > 0$ , $V_j = 0$ for $j > 1$

Within the simple Hubbard Hamiltonian the potential-energy contribution to the barrier to resonance originates in the energy required to create doubly occupied sites, as seen in Fig. 6. Once a doubly occupied site is created, both the cross or the dot can move freely and there is now only a kinetic-energy barrier to their motion. With a nonzero nearest-neighbor interaction the initial energy for creating a cross and a dot is  $\sim U - V_1$ , but there is now an additional potential-energy barrier that tends to localize the double occupancy and the hole. Referring back to Fig. 6, we see that the nearest-neighbor interaction imposes an additional barrier  $V_1$  at the second step in the path involving  $N_x = 1$ , at the third step in the path involving  $N_x = 2$ , etc. Indeed, this concept is closely related to the observation that an extended Hubbard Hamiltonian has *two* optical absorptions,<sup>52</sup> a strong intense peak at  $\sim U - V_1$  and a weaker secondary peak at  $\sim U$ . Thus a nonzero nearest-neighbor interaction is expected to strongly enhance the dimerization, and it should also be obvious that the dimerization here is far stronger than it is with an effective on-site correlation  $U_{\text{eff}}$ . Numerically, this has already been demonstrated by Hirsch<sup>14</sup> for  $U = 4t_0$ ,  $V_1 = 2t_0$ . Thus without even allowing for the modulation of  $V_1$  the ground state is strongly dimerized for  $V_1 > 0$ .

There is, however, an additional effect of the nearest-neighbor interaction on the ground-state wave function. The matrix element of  $H_{e-e}$  for the covalent diagrams is  $NV_1$  for a  $N$ -site periodic ring while that for the completely ionic configuration  $|VI\rangle$  in Fig. 3 is  $NU/2$ . Thus for  $V_1 > \frac{1}{2}U$  the ground state is dominated by the on-site CDW configurations in which alternate sites are doubly occupied. Since each doubly occupied site has a hole on both sides, these configurations strongly favor equal bond orders. The ground state has a different kind of charge ordering now and we expect a smooth reversal from a highly dimerized to a uniform system as  $V_1$  becomes larger than  $\frac{1}{2}U$ . This explains then why Hirsch finds such a large enhancement in dimerization for  $U = 4t_0$ ,  $V_1 = 2t_0$ , while a still larger  $V_1$  would have reduced the dimerization.

As in Sec. II, we again confirm the above predictions by numerical calculations. The  $N = 6$  and 10 results are again identical, so we present only the latter ones. The energies per site now converge slower than for the simple Hubbard Hamiltonian, but convergence is still much faster than in the SSH Hamiltonian, for which we have already shown that the energies per site have essentially converged at  $N = 10$ . Moreover, the enhancements in dimerization here are so large that finite-size effects are of no concern whatsoever, as shown below. We again calculate in each case the energy gained per site upon dimerization, defined exactly as in Eq. (11), but with a nonzero  $V_1$ . We have chosen  $\alpha^2/K$  the same as in Fig. 7(b), so that comparisons between simple and extended Hubbard Hamiltonians may be made readily. In Figs. 10(a)–10(c) we present our results for  $U/\sqrt{2}t_0 = 3, 5, \text{ and } 7$ , and for several values of  $V_1$  in each case, both  $V_1 < \frac{1}{2}U$  and  $V_1 > \frac{1}{2}U$ . The numerical results match our predictions completely, and the strong enhancement in dimerization

for  $V_1 < \frac{1}{2}U$  and the destruction of the dimerized state for  $V_1 > \frac{1}{2}U$  is obvious in each case. This very strong effect of  $V_1$  is most clear in Fig. 10(c), where even with a very large  $U$  the system is strongly dimerized for  $V_1/\sqrt{2}t_0=3$ . Comparison of Figs. 7(b) and 10 also indicates that dimerization within an extended Hubbard Hamiltonian cannot be described by an effective on-site repulsion  $U_{\text{eff}}=U-V_1$ . This is seen most clearly in Fig. 10(a), where the dimerization with  $U/\sqrt{2}t_0=3, V_1/\sqrt{2}t_0=1$  is stronger than with  $U/\sqrt{2}t_0=3, V_1=0$ , while the dimerization for  $U/\sqrt{2}t_0=1, V_1=0$  is weaker than that obtained with  $U/\sqrt{2}t_0=3, V_1=0$ . On the other hand, the system is undimerized for  $U/\sqrt{2}t_0=3, V_1/\sqrt{2}t_0=2$ , but is dimerized for  $U/\sqrt{2}t_0=1, V_1=0$ . Similarly, for fixed values of  $U-V_1$ ,  $U/\sqrt{2}t_0=5, V_1/\sqrt{2}t_0=2$ , and

$U/\sqrt{2}t_0=7, V_1/\sqrt{2}t_0=4$ , for instance, the behavior of the system is seen to be completely different. This particular feature of the extended Hubbard Hamiltonian is common to all values of  $U$  and  $V_1$ , and the reason has already been given. We emphasize, however, that this is a characteristic of the ground-state dimerization only, and the lowest excitations for the case of  $V_1 < \frac{1}{2}U$  can still be described by  $U_{\text{eff}} \sim U - V_1$ . This is particularly true of spin excitations,<sup>53</sup> and also for the optical absorptions,<sup>52</sup> in which the main peak occurs at  $\sim U - V_1$ .

Comparing the actual electronic energies it is simple in this case to ascertain that finite-size effects here are insignificant. We define  $\Delta E_{\text{el}}(U, V_1, N, \alpha x)$  as the difference in electronic energies per site between dimerized and uniform ring of  $N$  sites for fixed dimerization  $\alpha x$ , i.e.,

$$\Delta E_{\text{el}}(U, V_1, N, \alpha x) = \frac{1}{Nt_0} [E_{\text{el}}(U, V_1, N, \alpha x) - E_{\text{el}}(U, V_1, N, 0)], \quad (12)$$

and observe that  $|\Delta E_{\text{el}}|$  increases with  $N$  for arbitrary  $U$  and  $V_1$ . For the SSH Hamiltonian, we compute  $\Delta E_{\text{el}}$  for  $N=102$ , where ground-state electronic energies per site have converged at all  $\alpha x$ . For  $\alpha x=0.1$ , the region near where the curves in Fig. 10 exhibit minima,  $|\Delta E_{\text{el}}(N=102)|=0.064100$  for the SSH Hamiltonian. For the extended Hamiltonian,

$$|\Delta E_{\text{el}}(U=3\sqrt{2}t_0, V_1=\sqrt{2}t_0, N=10, \alpha x=0.1)| = 0.073047,$$

while

$$|\Delta E_{\text{el}}(U=5\sqrt{2}t_0, V_1=2\sqrt{2}t_0, N=10, \alpha x=0.1)| = 0.073338,$$

so that even the 10-site extended Hubbard ring is more strongly dimerized than the infinite SSH ring. Thus for the extended Hubbard Hamiltonian, the dimerizations are so strong that finite-size effects are absolutely unimportant.

With a periodic variation in  $V_1$ , as suggested by Whangbo,<sup>9</sup>  $V_1 = \bar{V}_1(1 \pm 2\lambda x)$ , where  $\lambda$  is a second electron-phonon coupling constant, dimerization can only be expected to be further enhanced. Considering any sequence of three singly occupied sites, charge transfer along the shorter bond now costs  $\sim U - \bar{V}_1(1 + 2\lambda x)$  while the energy required for charge transfer along the longer bond is  $\sim U - \bar{V}_1(1 - 2\lambda x)$ . Thus bond-order differences become larger and the enhancement in dimerization should increase with  $\lambda$ . We demonstrate this in Fig. 11(a), for  $\bar{V}_1 < \frac{1}{2}U$ , and in Fig. 11(b), for  $\bar{V}_1 > \frac{1}{2}U$  for several values of  $\lambda/\alpha$ . For a very large  $\lambda$  the on-site CDW in Fig. 11(b) can be destroyed and dimerization can be restored again. We note, however, that as seen from our previous results, a large nonzero  $\lambda$  is not a necessary condition for dimerization.

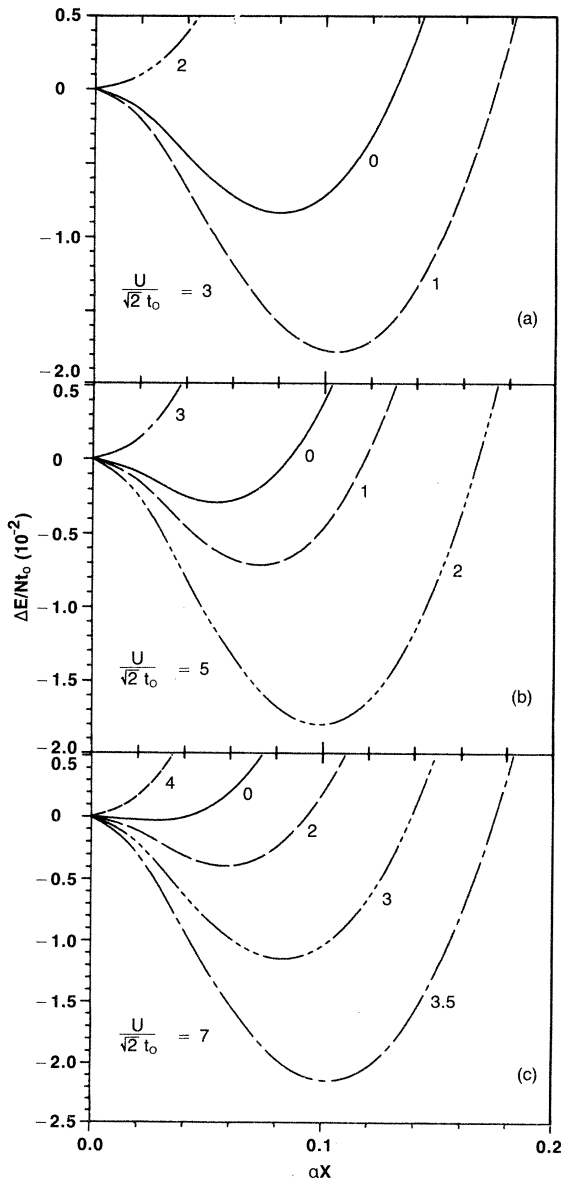


FIG. 10. Energy gained per electron on dimerization for  $N=10$  and  $U \neq 0, V_1 \neq 0, V_2=0$ . Numbers on each curve are the different values of  $V_1/\sqrt{2}t_0$ . Magnitude of  $K/\alpha^2$  is the same as in Fig. 7(b).

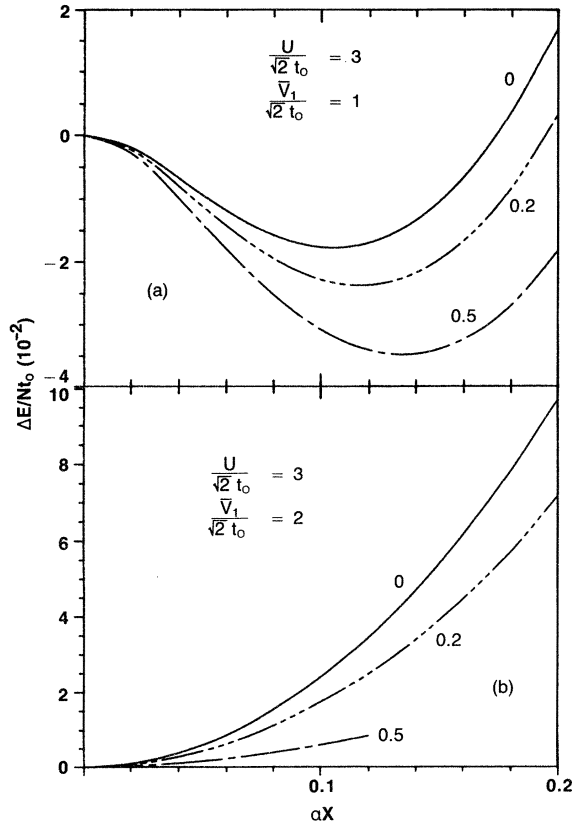


FIG. 11. Same as in Fig. 10 except  $V_1 = \bar{V}_1(1 \pm 2\lambda x)$  here. Numbers on each curve are the magnitudes of  $\lambda/\alpha$ .

### B. $V_1, V_2 > 0$ , $U \geq 2V_1$ , $V_j = 0$ for $j > 2$

We now discuss the effect of the second-neighbor interaction. We discuss the two regions  $V_1 < \frac{1}{2}U$  and  $V_1 > \frac{1}{2}U$  separately, as the effect of  $V_2$  is drastically different in the two cases. We go back to Fig. 6 and consider the barrier to resonance for  $V_2 > 0$ . Within the path involving  $N_x = 1$ , the barrier to the first step is still  $\sim U - V_1$ , but the barrier to the second step is  $\sim V_1 - V_2$ . The third step, which did not have any potential-energy barrier before now costs an additional energy  $V_2$ , and exactly in analogy with the effect of  $V_1$  we might therefore be led to believe that  $V_2$  further enhances the dimerization. This is not true, however, even though  $V_2$  tends to localize the single pair of cross and dot. The reason can be seen by analyzing paths involving slightly larger  $N_x$ . Now the barrier is  $V_1 - V_2$  in the third step for  $N_x = 2$ , in the fourth step for  $N_x = 3$ , etc., i.e., in the  $N_x + 1$  step for the path involving  $N_x$  doubly occupied sites. Dimerization would increase with  $V_2 > 0$  if in the immediate next step the barrier is  $V_2$ , since otherwise, starting from any one Kekulé structure, it becomes easier to reach more near the centers of the paths. The barrier in the  $(N_x + 2)$ th step, as may be seen by careful analysis of the indirect interaction between any pair of doubly occupied sites, is  $V_2$  only when the distance between the nearest pair of crosses is greater than nine atomic sites. Thus in all paths involving  $N_x \geq 0.1N$ , the  $(N_x + 1)$ th step, which previously had a

barrier  $V_1$ , now has a barrier  $V_1 - V_2$  but the  $(N_x + 2)$ th step has a barrier 0. Only at a much later step is the diagonal energy of  $V_2$  regained, so that the contribution of diagrams which favor a BOW increases only weakly with  $V_2$ . In a large system then, the barrier to resonance increases for paths involving  $N_x \leq 0.1N$ , but decreases for paths involving  $N_x \geq 0.1N$ . We have confirmed this by drawing paths between the Kekulé structures similar to those in Fig. 6 for rings as large as  $N = 18$  and 22. A positive  $U$ , opposing double occupancy, causes paths involving  $N_x > 0.1N$  to become less and less probable. On the other hand, these paths are clearly much larger in number as the maximum value of  $N_x$  is  $N/2$  and the number of diagrams within any class peaks at  $N_x \sim N/4$ . Furthermore, a positive  $V_1$  increases the probability of double occupancy and in certain cases, even increases the tendency towards a CDW state. Considering these competing effects of  $V_2$  then, we come to the following conclusions. Firstly, any effect of  $V_2$  on the dimerization, compared to the large enhancement reached with  $V_1$ , is small. Secondly, since paths involving  $N_x \geq 0.1N$  are overwhelmingly larger in number,  $V_2 > 0$  will slightly decrease the dimerization. However, since the barrier  $V_2$  occurs for some distant step even in the latter class of paths, dimerization here should be slightly stronger than that with an effective nearest-neighbor interaction  $V_1 - V_2$ .

The numerical results for  $V_2 > 0, V_1 < \frac{1}{2}U$  are shown in Figs. 12(a)–12(c) for several values of  $U, V_1$ , and  $V_2$ . The energy gained upon dimerization,  $\Delta E$ , is defined as in Eq. (11) with a nonzero  $V_1$  and  $V_2$ , while the same value of  $\alpha^2/K$  is chosen as before. The effect of  $V_2$  is indeed found to be small, and a slight reduction in dimerization is seen to occur. Comparison of the results in Figs. 10 and 12 indicate, however, that the dimerization is stronger here than it is for an extended Hubbard Hamiltonian with an effective nearest-neighbor interaction  $V_1 - V_2$ . Thus from Figs. 10(b) and 12(b), dimerization is stronger for  $U/\sqrt{2}t_0 = 5, V_1/\sqrt{2}t_0 = 2, V_2/\sqrt{2}t_0 = 1$  than for  $U/\sqrt{2}t_0 = 5, V_1/\sqrt{2}t_0 = 1$ . Similarly the system is more strongly dimerized for  $U/\sqrt{2}t_0 = 7, V_1/\sqrt{2}t_0 = 3, V_2/\sqrt{2}t_0 = 1$  than it is for  $U/\sqrt{2}t_0 = 7, V_1/2t_0 = 2$ .

### C. $V_1, V_2 > 0$ , $U < 2V_1$ , $V_j = 0$ for $j > 2$ .

Unlike the previous case we expect here a rather drastic effect of nonzero  $V_2$ , and this is also a far simpler case. Recall that for  $V_1 > \frac{1}{2}U, V_2 = 0$ , the system has a strong tendency to have uniform bond order as the on-site CDW configurations are stabilized by these parameters. If we now include a  $V_2 > 0$ , the matrix elements of  $H_{e-e}$  for the covalent diagrams increase by  $NV_2$  while those for the two configurations that favor the CDW very strongly increases by  $2NV_2$ . A nonzero  $V_2$  then strongly destabilizes the configurations favoring a CDW, thereby increasing the contribution of diagrams that favor a BOW. Once this is reached, however, further increase in  $V_2$  only decreases the barrier to resonance between the Kekulé diagrams, as in the previous case. Thus the initial effect of  $V_2$  is to strongly enhance the dimerization, followed by a

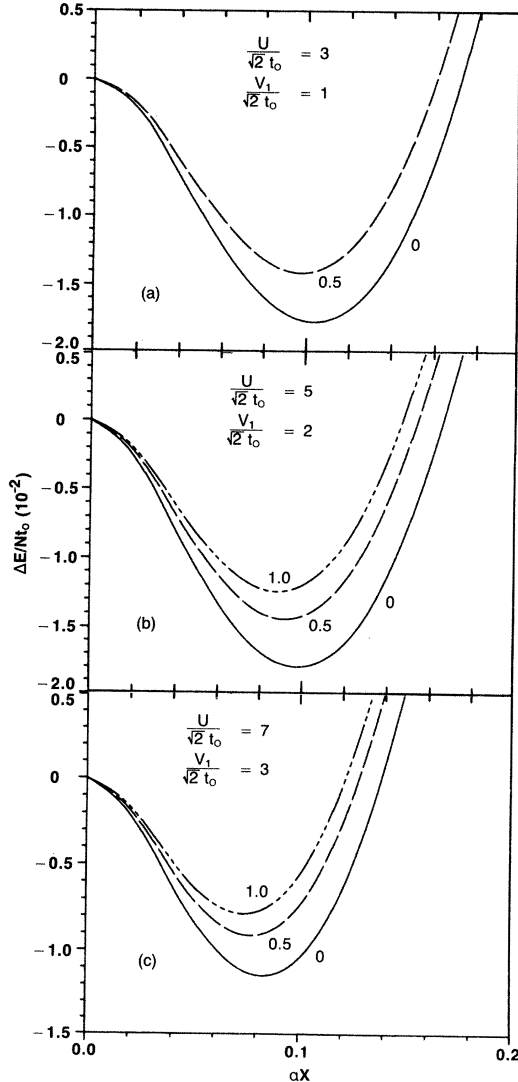


FIG. 12. Energy gained per electron on dimerization for  $N=10$  and  $V_1 < \frac{1}{2}U, V_2 \neq 0$  for several values of  $U$  and  $V_1$ . Numbers on each curve are the magnitudes of  $V_2/\sqrt{2}t_0$ . Magnitude of  $K/\alpha^2$  is same as before.

smooth reduction in the dimerization, and for reasonable values of  $U, V_1$  and  $V_2$  dimerization remains enhanced compared to the SSH Hamiltonian.

The numerical results for this case are presented in Figs. 13(a)–13(c). The values of  $U$  chosen here are the same as those in Fig. 12, but in each case we have chosen  $V_1 > \frac{1}{2}U$ . While  $V_2=0$  gives a strongly undimerized state, a very small nonzero  $V_2$  gives a rather large dimerization here, while further increase in  $V_2$  decreases the dimerization. Again, relative to the SSH Hamiltonian, dimerization remains enhanced for a wide range of parameters. Comparison to Fig. 10 indicates that  $\Delta E_{el}$  here is again much too large for finite-size effects to be of any importance, so that the enhancement in dimerization compared to the SSH Hamiltonian is real and would persist for arbitrary  $N$ .

To demonstrate the large and sudden change in the nature of the wave function in this case we present the total

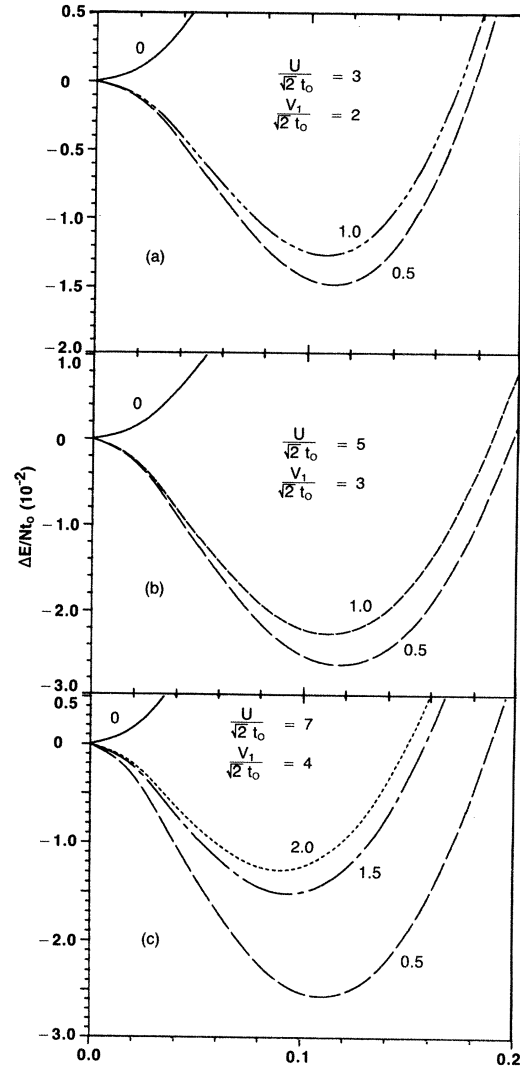


FIG. 13. Same as in Fig. 12 for  $V_1 > \frac{1}{2}U$ .

normalized contributions of the various classes of diagrams to the undimerized ground-state wave functions for  $U/\sqrt{2}t_0=5, V_1/\sqrt{2}t_0=3$  and several values of  $V_2$  in Fig. 14, which is to be compared with Fig. 9. For  $V_2=0$ , the ground-state contribution is largest for the class of diagrams with  $N_x=N/2$ , as indeed would be expected for a CDW ground state. For  $V_2>0$ , the nature of the wave function changes drastically and diagrams with small  $N_x$  now dominate the ground state. As in Fig. 9, this shift in the peaks of the curves towards smaller  $N_x$  is a signature of the enhanced dimerization for these correlation parameters in the presence of nonzero  $\alpha$ . The shift towards smaller  $N_x$  implies greater contribution by diagrams with large  $|\delta|$  and a positive potential-energy contribution to the barrier to resonance. We have presented the above change in the ground-state wave function for only one representative case, but the results are similar for all  $U, V_1, V_2$ . We shall indicate below how this information can be used to predict the nature of the ground state of the PPP Hamiltonian.

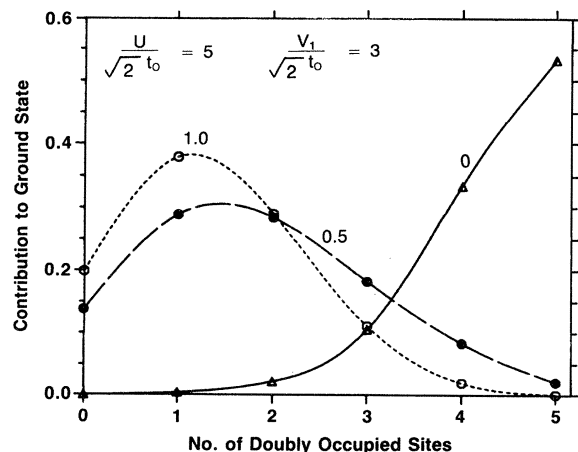


FIG. 14. Same as in Fig. 9 for  $U/\sqrt{2}t_0=5$ ,  $V_1/\sqrt{2}t_0=3$ . Numbers on each curve are the different values of  $V_2/\sqrt{2}t_0$ .

#### D. PPP Hamiltonian

In principle, our physical arguments can be extended to include arbitrarily long-range interactions, but in practice it soon becomes extremely complicated. Even for the paths involving  $N_x=1$  we have to consider the  $j$ th step from the initial Kekulé diagram for a nonzero  $V_j$ . Thus the requirement for  $j$ , for both a correct prediction from the physical arguments and for numerical results free of finite-size effects, is that  $j < N/2$ . For any larger  $j$ , finite-size effects become important. To consider long-range interactions then, we should deal with larger and larger systems. We point out here that this is in fact not necessary, and a sequence of logical reasonings based on our results and some additional experimental and theoretical information leads to the conclusion that the ground state in the PPP Hamiltonian is dimerized for both the Mataga-Nishimoto and Ohno parameters. These reasonings are as follows.

We have seen that for a correlated band there are three different kinds of broken symmetry: the pure SDW with uniform bond order, the dimerized BOW state, and the on-site CDW state. Dimerization begins to decrease only after the covalent diagrams begin to dominate the ground-state wave function. Within the PPP Hamiltonian,  $U \sim 4t_0$ , the region where dimerization is the largest. Finite intersite interactions can only reduce the magnitude of the effective spin-exchange integral, so that the pure SDW state is not possible for the PPP Hamiltonian. On the other hand, the CDW state requires larger contribution from diagrams with  $N_x > N/4$  than from diagrams with  $N_x < N/4$ , i.e., the peak in the contribution curve has to be on the *right* of the SSH curve in Fig. 9. In this

sense, the CDW state is a “negative- $U_{\text{eff}}$  state. However, this kind of a ground-state wave function cannot have the  $^1A_g$  state as the lowest excited state or negative spin densities. Since the PPP Hamiltonian reproduces the above properties for long polyenes, the ground state of the PPP Hamiltonian must have a larger contribution from diagrams with  $N_x < N/4$  than the ground state of the SSH Hamiltonian. The peak in the contribution curve for the PPP Hamiltonian is then to the *left* of the SSH curve in Fig. 9, and the ground state is a “positive- $U_{\text{eff}}$ ” state. We conclude therefore that our results strongly indicate that the ground state is dimerized for the PPP Hamiltonian, as neither the SDW nor the CDW state is possible, and the infinite ring will always have some kind of broken symmetry due to the infinitely long paths between appropriate pairs of configurations.

#### V. CONCLUSIONS

We have investigated the effects of electron-electron interactions on dimerization in a half-filled band within a novel real-space approach. Dimerization in a correlated band is shown to be a result of imperfect resonance rather than of opening a gap in the single-particle density of states. The one-electron picture of Peierls is a special case valid only for the SSH limit. Contrary to previous predictions, the Hubbard on-site interaction is found to strongly enhance the dimerization. Inclusion of intersite interactions further enhances the dimerization, except in the case of  $V_1 > \frac{1}{2}U$ ,  $V_2=0$ . The gain in electronic energy on dimerization when intersite interactions are included can be so large that  $\Delta E_{\text{el}}(N=10)$  in these cases are larger than  $\Delta E_{\text{el}}(N \rightarrow \infty)$  for the SSH limit. For the PPP Hamiltonian we conclude that the above results strongly indicate that the ground is dimerized. Existence of dimerization in polyacetylene thus does not prove that electron-electron interactions are weak in this material. The magnitudes of the correlation parameters can only be determined from other measurements, and accurate estimates of the various parameters are required for a more precise description of the ground and excited states in polyacetylene. The effect of electron correlations on the solitonlike and polaronlike states in this material is of interest, and research is in progress.

#### ACKNOWLEDGMENTS

The current work would not have been possible without the continuing encouragement of Dr. D. K. Campbell. One of us (S.M.) acknowledges useful discussions with Dr. A. R. Bishop, Dr. D. K. Campbell, and Professor Z. G. Soos. Work at Los Alamos National Laboratory was supported by the U. S. Department of Energy.

\* Present address: Noyes Laboratory for Chemical Physics, California Institute of Technology, Pasadena, CA 91125.

<sup>1</sup>R. E. Peierls, *Quantum Theory of Solids* (Clarendon, Oxford, 1955), Chap. 5.

<sup>2</sup>N. A. Popov, *Zh. Strukt. Khim.* **10**, 533 (1969).

<sup>3</sup>A. Madhukar, *Solid State Commun.* **15**, 921 (1974).

<sup>4</sup>A. A. Ovchinnikov, I. I. Ukrainskii and G. V. Kventselev, *Usp. Fiz. Nauk.* **108**, 51 (1972) [*Sov. Phys.—Usp.* **15**, 575 (1973)].

- <sup>5</sup>I. Egri, *Z. Phys. B* **23**, 381 (1976); *Solid State Commun.* **22**, 281 (1977).
- <sup>6</sup>I. Ukrainskii, *Zh. Eksp. Teor. Fiz.* **76**, 760 (1979) [*Sov. Phys.—JETP* **49**, 381 (1979)].
- <sup>7</sup>K. R. Subbaswamy and M. Grabowski, *Phys. Rev. B* **24**, 2168 (1981).
- <sup>8</sup>P. Horsch, *Phys. Rev. B* **24**, 7351 (1981).
- <sup>9</sup>M. Whangbo, *J. Chem. Phys.* **75**, 2983 (1981).
- <sup>10</sup>H. Fukutome and M. Sasai, *Prog. Theor. Phys.* **67**, 41 (1982).
- <sup>11</sup>S. Kivelson and D. Heim, *Phys. Rev. B* **26**, 4278 (1982).
- <sup>12</sup>H. T. Jonkman, S. Huizinga, and J. Kommandeur, *Mol. Cryst. Liq. Cryst.* **95**, 165 (1983).
- <sup>13</sup>S. Mazumdar and S. N. Dixit, *Phys. Rev. Lett.* **51**, 292 (1983).
- <sup>14</sup>J. E. Hirsch, *Phys. Rev. Lett.* **51**, 296 (1983).
- <sup>15</sup>See for example, *Proceedings of the International Conference on the Physics and Chemistry of Conducting Polymers*, Les Arcs, France, 1982 [*J. Phys. (Paris)* (in press)].
- <sup>16</sup>W. P. Su, J. R. Schrieffer, and A. J. Heeger, *Phys. Rev. Lett.* **42**, 1698 (1979); *Phys. Rev. B* **22**, 2099 (1980); *B* **28**, 1138(E) (1983).
- <sup>17</sup>M. J. Rice, *Phys. Lett.* **71A**, 152 (1979); M. J. Rice and J. Timonen, *ibid.* **73A**, 368 (1979).
- <sup>18</sup>S. A. Brazovskii, *Zh. Eksp. Teor. Fiz. Pis'ma Red* **28**, 656 (1978) [*JETP Lett.* **28**, 606 (1978)]; [*Sov. Phys.—JETP* **51**, 342 (1980)]; S. A. Brazovskii and N. Kirova, *Zh. Eksp. Teor. Fiz. Pis'ma Red* **33**, 6 (1981) [*JETP Lett.* **33**, 4 (1981)].
- <sup>19</sup>H. Takayama, Y. R. Lin-Liu, and K. Maki, *Phys. Rev. B* **21**, 2388 (1980).
- <sup>20</sup>J. A. Krumhansl, B. Horovitz, and A. J. Heeger, *Solid State Commun.* **34**, 945 (1980).
- <sup>21</sup>D. K. Campbell and A. R. Bishop, *Phys. Rev. B* **24**, 4859 (1981); D. K. Campbell, A. R. Bishop, and K. Feeser, *ibid.* **26**, 6862 (1982).
- <sup>22</sup>B. Horovitz, *Phys. Rev. Lett.* **46**, 742 (1981).
- <sup>23</sup>H. Kuhn, *Helv. Chim. Acta* **31**, 1441 (1948).
- <sup>24</sup>C. A. Coulson, *Proc. R. Soc. London Ser. A* **164**, 383 (1938).
- <sup>25</sup>H. Labhart, *J. Chem. Phys.* **27**, 957 (1957).
- <sup>26</sup>Y. Ooshika, *J. Phys. Soc. Jpn.* **12**, 1246 (1957).
- <sup>27</sup>H. C. Longuet-Higgins and L. Salem, *Proc. R. Soc. London Ser. A* **25**, 172 (1959).
- <sup>28</sup>C. A. Coulson and W. T. Dixon, *Tetrahedron* **17**, 215 (1961).
- <sup>29</sup>J. A. Pople and S. H. Walmsley, *Mol. Phys.* **5**, 15 (1962).
- <sup>30</sup>A. Karpfen and J. Petkov, *Theor. Chim. Acta* **53**, 65 (1979), and references therein. See also J. L. Bredas, R. R. Chance, R. Silbey, G. Nicholas, and Ph. Durand, *J. Chem. Phys.* **75**, 255 (1981), and references therein.
- <sup>31</sup>T. Nakano and H. Fukuyama, *J. Phys. Soc. Jpn.* **49**, 1679 (1980).
- <sup>32</sup>S. Ramasesha and Z. G. Soos, *Int. J. Quant. Chem.* (to be published).
- <sup>33(a)</sup>C. R. Fincher, Jr., C. E. Chen, A. J. Heeger, and A. G. MacDiarmid, *Phys. Rev. Lett.* **48**, 100 (1982); (b) T. C. Clarke *et al.*, in *Proceedings of the International Conference on the Physics and Chemistry of Conducting Polymers*, Les Arcs, France, 1982, Ref. 15; *Phys. Rev. Lett.* **51**, 1191 (1983).
- <sup>34</sup>R. M. Gavin, Jr., C. Weisman, J. M. McVey, and S. A. Rice, *J. Chem. Phys.* **68**, 522 (1978); M. F. Granville, G. R. Holtom, and B. E. Kohler, *ibid.* **72**, 4671 (1980).
- <sup>35</sup>B. S. Hudson, B. E. Kohler, and K. Schulten, in *Excited States*, edited by E. C. Lim (Academic, New York, 1982), Vol. 6, and references therein.
- <sup>36</sup>I. Ohmine, M. Karplus, and K. Schulten, *J. Chem. Phys.* **68**, 2298 (1978).
- <sup>37</sup>L. R. Ducasse, T. E. Miller, and Z. G. Soos, *J. Chem. Phys.* **76**, 4094 (1982); Z. G. Soos and S. Ramasesha, *Chem. Phys. Lett.* **101**, 34 (1983).
- <sup>38</sup>J. Cizek, J. Paldus, and L. Srobkova, *Int. J. Quant. Chem.* **III**, 149 (1969); J. Paldus and J. Cizek, *ibid.* **XV**, 463 (1979); *J. Polymer Sci., Part C*, **29**, 199 (1970).
- <sup>39</sup>J. Paldus and M. J. Boyle, *Int. J. Quant. Chem.* **XXII**, 1281 (1982).
- <sup>40</sup>F. A. Matsen, *Acc. Chem. Res.* **11**, 387 (1978).
- <sup>41</sup>B. Honig, A. Warshel, and M. Karplus, *Acc. Chem. Res.* **8**, 92 (1975), and references therein.
- <sup>42</sup>H. Thomann, L. R. Dalton, Y. Tomkiewicz, N. S. Shiren, and T. C. Clarke, in *Proceedings of the International Conference on the Physics and Chemistry of Conducting Polymers*, Les Arcs, France, 1982, Ref. 15, and unpublished.
- <sup>43</sup>M. W. Hanna, A. D. McLachlan, H. H. Dearman, and H. M. McConnell, *J. Chem. Phys.* **37**, 361 (1962).
- <sup>44</sup>H. M. McConnell and D. B. Chesnut, *J. Chem. Phys.* **27**, 984 (1957); A. D. McLachlan, *Mol. Phys.* **2**, 223 (1959); see also M. Thomas Jones *et al.*, in *Proceedings of the International Conference on the Physics and Chemistry of Conducting Polymers*, Les Arcs, France, 1982, Ref. 15.
- <sup>45</sup>S. T. Chui, T. M. Rice, and C. M. Varma, *Solid State Commun.* **15**, 575 (1973).
- <sup>46</sup>E. Lieb and F. Y. Wu, *Phys. Rev. Lett.* **20**, 1445 (1968); H. Shiba, *Phys. Rev. B* **6**, 930 (1972).
- <sup>47</sup>S. Mazumdar and S. N. Dixit, *Phys. Rev. B* (in press).
- <sup>48</sup>M. J. Rice and E. J. Mele, *Phys. Rev. Lett.* **49**, 1455 (1982).
- <sup>49</sup>S. Mazumdar and Z. G. Soos, *Synth. Met.* **1**, 77 (1979).
- <sup>50</sup>S. Huizinga, J. Kommandeur, H. T. Jonkman, and C. Haas, *Phys. Rev. B* **25**, 1717 (1982).
- <sup>51</sup>P. W. Anderson, *Phys. Rev.* **86**, 694 (1952).
- <sup>52</sup>S. Mazumdar and Z. G. Soos, *Phys. Rev. B* **23**, 2810 (1981).
- <sup>53</sup>S. Mazumdar and A. N. Bloch, *Phys. Rev. Lett.* **50**, 207 (1983), and unpublished.